Acta Geochim (2024) 43:661–676
https://doi.org/10.1007/s11631-024-00709-y

ORIGINAL ARTICLE

Rebuilding the theory of isotope fractionation for evaporation of silicate melts under vacuum condition

Jie Wang[1,2] · **Yun Liu**[1,2,3]

Received: 13 May 2024 / Revised: 20 May 2024 / Accepted: 27 May 2024 / Published online: 14 June 2024

Abstract Isotope effects are pivotal in understanding silicate melt evaporation and planetary accretion processes. Based on the Hertz–Knudsen equation, the current theory often fails to predict observed isotope fractionations of laboratory experiments due to its oversimplified assumptions. Here, we point out that the Hertz-Knudsen-equation-based theory is incomplete for silicate melt evaporation cases and can only be used for situations where the vaporized species is identical to the one in the melt. We propose a new model designed for silicate melt evaporation under vacuum. Our model considers multiple steps including mass transfer, chemical reaction, and nucleation. Our derivations reveal a kinetic isotopic fractionation factor (KIFF or α) $\alpha_{\text{our model}} = [m(^1\text{species})/m(^2\text{species})]^{0.5}$, where m(species) is the mass of the reactant of reaction/nucleation-limiting step or species of diffusion-limiting step and superscript 1 and 2 represent light and heavy isotopes, respectively. This model can effectively reproduce most reported KIFFs of laboratory experiments for various elements, i.e., Mg, Si, K, Rb, Fe, Ca, and Ti. And, the KIFF-mixing model referring that an overall rate of evaporation can be determined by two steps jointly can account for the effects of low P_{H2} pressure, composition, and temperature. In addition, we find that chemical reactions, diffusion, and nucleation can control the overall rate of evaporation of silicate melts by using the fitting slope in $\ln(-\ln f)$ versus $\ln(t)$. Notably, our model allows for the theoretical calculations of parameters like activation energy (E_a), providing a novel approach to studying compositional and environmental effects on evaporation processes, and shedding light on the formation and evolution of the proto-solar and Earth-Moon systems.

Keywords Evaporation · Kinetic isotopic fractionation · Chemical kinetics · Hertz–Knudsen equation · CAIS

1 Introduction

Evaporation process can significantly change the isotopic composition of an object. Refractory calcium-aluminum-rich inclusions (CAIs) are the oldest silicate solids formed in the solar system (Connelly et al. 2012) and have experienced high-temperature evaporation processes (Grossman et al. 2000, 2008). Therefore, CAIs have been used to investigate how the proto-solar system forms and evolves. Consequently, many evaporation experiments of silicate melts were designed to measure the kinetic isotope fractionations for various isotope systems, e.g., Mg, K, Ca, Ti, Si, and so on. All silicate residues under vacuum showed significant heavy isotope enrichments compared to their starting materials (e.g., Wang et al. 2001; Richter et al. 2002; Knight et al. 2009; Mendybaev et al. 2021).

A theory based on the Hertz–Knudsen equation (H–K equation hereafter) (e.g., Hirth and Pound 1963) was first proposed by Richter et al. (2002) to explain isotope fractionations during the evaporation process. The Rayleigh distillation model was also incorporated into the theoretical treatment to predict the kinetic isotope fractionation factor (KIFF) (Richter et al. 2002, 2004). They concluded

✉ Yun Liu
liuyun@vip.gyig.ac.cn

[1] Research Center for Planetary Science, College of Earth and Planetary Sciences, Chengdu University of Technology, Chengdu 610059, China

[2] State Key Laboratory of Ore Deposit Geochemistry, Institute of Geochemistry, Chinese Academy of Sciences, Guiyang 550081, China

[3] CAS Center for Excellence in Comparative Planetology, Hefei 230026, China

that the calculated KIFFs based on the H–K equation only depend on the molecular mass ratio of gaseous species, i.e., $\alpha_{HK}=(m_1/m_2)^{0.5}$, where subscript 1 or 2 indicates their molecular mass with light or heavy isotope (Richter et al. 2002, 2004). Since then, the H–K equation has been widely used in the study of evaporation/condensation processes in the communities of geosciences and planetary sciences (e.g., Wang and Jacobsen 2016; Hu et al. 2021; Nie et al. 2021).

However, there is a clear inconsistency between the theoretically predicted results based on the H–K equation and the experimental ones. For example, for Mg evaporation experiments, the compositions of silicate melts can be divided into two types, i.e., melilitic melt and forsteritic melt (Mendybaev et al. 2013a, b, 2021). The experimental KIFF for Mg of melilitic melt is 0.9870 ± 0.0002 (Richter et al. 2007) or 0.9877 ± 0.0004 (Mendybaev et al. 2021). Meanwhile, for the forsteritic melt, the experimental KIFF is about 0.9840 (Davis et al. 1990; Mendybaev et al. 2013a, b). However, the experimental evidence suggested that the vaporized species of those silicate melts is an Mg atom (Shornikov and Yakovlev 2015). According to the H–K-equation-based theory, the fractionation factor is $\alpha^{25}_{Mg,HK}$=0.9798. This KIFF is different from the experimental results (Fig. 3). Another example is the silicon (Si) isotope system and the experimental KIFF for Si is 0.9898 ± 0.0004 (Knight et al. 2009), 0.9928 ± 0.0002 (Davis et al. 1990) or 0.9910 ± 0.0005 (Mendybaev et al. 2021), but the theoretical KIFF is $\alpha^{29}_{SiO,HK}=0.9917$(Fig. 4) since the dominant vaporized species is found as SiO.

Meanwhile, there are some predictions based on the H–K equation that do match the experimental results very well. For example, the experimental KIFF is 0.9812 ± 0.0004 for Fe in wüstite (pure FeO) melt (Dauphas et al. 2004), 0.9748 ± 0.0012 at 1200 °C for K (Zhang et al. 2021) and 0.9562 for Ca in perovskite ($CaTiO_3$) (Zhang et al. 2014), then they are close to the results based on the H–K equation, i.e., $\alpha^{56}_{Fe,HK}=0.9820$, $\alpha^{41}_{K,HK}=0.9753$ and $\alpha^{44}_{Ca,HK}=0.9535$ (Fig. 5), respectively.

Note that the reported gas pressure also can significantly change the evaporation results (e.g., Wimpenny et al. 2019; Sossi et al. 2020; Badro et al. 2021). However, we focus on the simplest situation here, i.e., the evaporation occurs under vacuum conditions. On the other hand, how to interpret both mismatching and matching results? It could be explained if we change the vaporized gas species to other forms (Davis et al. 1990; Wang et al. 2001; Mendybaev et al. 2021). For example, Magnesium escapes melt as MgO instead of Mg species, but it is not supported by experiments and calculations (Fedkin et al. 2006; Shornikov and Yakovlev 2015).

In this study, we point out that under ideal vacuum conditions, the H–K-equation-based theory is improper for silicate melt cases. Then we rebuild the isotope fractionation theory for the evaporation of silicate melts in vacuum by introducing the mass transfer, reaction, and nucleation steps.

2 Methods

2.1 The H–K-equation-based isotope fractionation theory

The essence of the H–K equation is its clear expression of the evaporation flux (Hirth and Pound 1963):

$$J_i^e=\frac{\gamma_i P_{i,sat}}{\sqrt{2\pi m_i RT}} \tag{1}$$

where J_i^e is the evaporation flux of i in moles per unit second per unit area and it represents the rate of collision with the gas–melt interface for gaseous species containing i, γ_i is the evaporation coefficient of i, $P_{i,sat}$ is the saturation vapor pressure of i, m_i is the molecular mass of gaseous species containing i, R is the gas constant, T is temperature in Kelvin.

The H–K equation was applied to calculate isotope fractionations for evaporation of silicate melts, usually coupling with the Rayleigh distillation model (Richter et al. 2002, 2004):

$$\frac{R_{2,1}}{R_0}=\left(\frac{X_1}{X_{0,1}}\right)^{\alpha-1} \tag{2}$$

$$\ln\left(\frac{R_{2,1}}{R_0}\right)=-(1-\alpha)\ln f \tag{3}$$

where α is the KIFF and $\alpha=\frac{\gamma_2 P_{2,sat}}{\gamma_1 P_{1,sat}}\sqrt{\frac{m_1}{m_2}}$; $f=\frac{X_1}{X_{0,1}}$; $R_{2,1}$ is the ratio of heavy and light isotopes of a given element i, m_1 and m_2 are the molecular masses of the gaseous species with light and heavy isotopes; X_1 and X_2 are the mole fractions of light and heavy isotopes in the evaporation residue, respectively; R_0 is the ratio of heavy and light isotopes, $\frac{X_{0,2}}{X_{0,1}}$, in starting materials where $X_{0,1}$ and $X_{0,2}$ are the moles of light and heavy isotopes, respectively; f is the fraction of the residue melt. Besides, Eq. (3) indicates an experimental methodology to obtain KIFF; further details can be found in Richter et al. (2002, 2007).

For solving $\alpha=\frac{\gamma_2 P_{2,sat}}{\gamma_1 P_{1,sat}}\sqrt{\frac{m_1}{m_2}}$, usually it is assumed that $\frac{\gamma_2}{\gamma_1}$ equals to 1. Bourdon and Fitoussi (2020) found that the evaporation coefficient is a function of temperature and their ratio should be close to 1 if under sufficiently high temperature, so neglecting the isotope effect of evaporation coefficients is reasonable because the studied silicate melts are

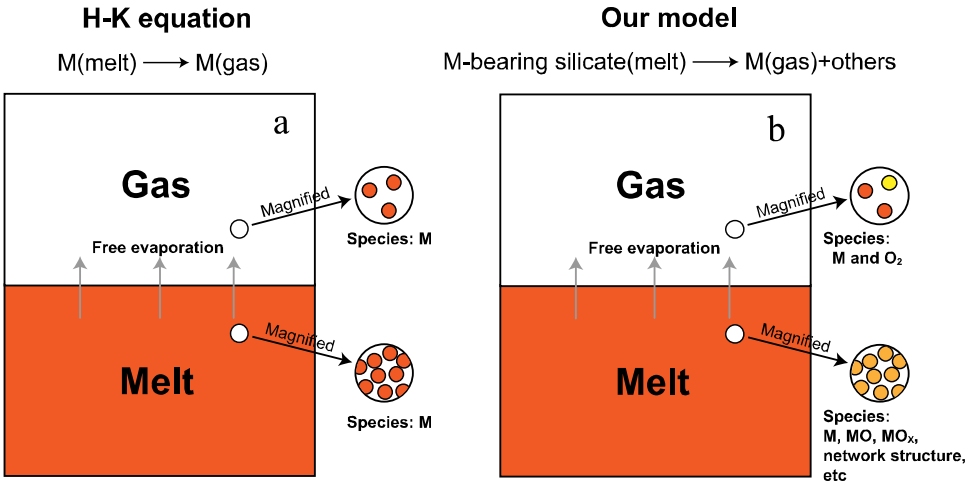

Fig. 1 Schematic diagram of **a** the H–K equation and **b** our model for free evaporation. The circles to the right of square represent the magnified structure at atomistic level. Circles with different colors represent different species

under high temperatures. Therefore, $\alpha = \alpha^{eq}\sqrt{\frac{m_1}{m_2}}$ by rewriting the ratio of partial saturation pressure into equilibrium isotope fractionation factor α^{eq}, if it is under sufficient high-temperature conditions (Bigeleisen 1961). Another assumption is that α^{eq} can be treated approximately as 1 if under high temperature suggested by classical isotope fractionation theory (Urey 1947; Bigeleisen and Mayer 1947). For Mg-bearing silicate melt evaporation at 1673 K, $\alpha^{eq} = 0.99989$ from the experiment (Richter et al. 2002) and $\alpha^{eq} = 0.99969$ from first-principles calculations (Luo et al. 2018). Therefore, it can be safely assumed that $\alpha^{eq} \approx 1$ under sufficient high temperatures. Consequently, the KIFF becomes $\alpha_{\mathrm{HK}} \approx \sqrt{\frac{m_1}{m_2}}$, which is a simple and beautiful equation derived from the H–K equation, where m_1 and m_2 are the molecular mass of vaporized species with light and heavy isotopes, respectively (Richter et al. 2002, 2007; Richter 2004; Knight et al. 2009; Mendybaev et al. 2021).

Theoretically, the H–K equation can be used to study the evaporation flux, the frequency of collision of a species crossing the interface between gas and solution/melt (Hertz 1882; Knudsen 1909; Langmuir and Irving 1913). However, practically the H–K equation can be used only under these conditions when (i) the pressure of a system is sufficiently low so that there is no recondensation process, (ii) the surface of melt is not contaminated with species that may retard the removal of gaseous species and (iii) the composition of the vaporizing species is the same as one in the melt (Hayes 2014). The prerequisite of the H–K equation, i.e., its rate is maximum in vacuum when its evaporation coefficient is unit, will be destructed if conditions (i) and (ii) are not met. And we can get its expression via a more readily process, i.e., the condensation of gases can be described well with the kinetic theory of gases (Kennard 1938). Importantly, it leads to that the species of both sides must be the same (Fig. 1a), which is the condition (iii).

Silicate melts contain complicated network structures consisting of different oxides, e.g., SiO_2, MgO, CaO, Al_2O_3, and K_2O, however, vaporized species are small molecules, e.g., Mg(g), MgO(gas), SiO (gas), SiO_2 (gas), O_2, and other complex molecules (Shornikov and Yakovlev 2015). In other words, the decomposition process may take place, and taking Mg as an example, it is Mg-bearing silicate → Mg(gas) instead of Mg(melt) → Mg(gas) for the H–K equation. Therefore, we propose that the H–K equation may not be suitable for the evaporation process of silicate melts, since the composition of silicate melt is not identical to gas species (Fig. 1b). Maybe it is the reason that causes disparities existing between experiments of silicate evaporation and KIFF predicted by the H–K equation. For situations of Fig. 1b, we present a better model or theory that can overcome the shortage of the H–K equation.

2.2 Our model

2.2.1 Theoretical foundation

Here we present a model to describe the evaporation of silicate melts. Before that, some assumptions must be given: (i) the rate of an evaporation process is controlled by chemical reactions, mass transfer, and nucleation processes; (ii) the overall rate of evaporation is dominated by the rate-limiting step. As a result, more details can be deduced via these two prerequisites with heterogeneous reactions where Phase I and II represent melt and gas phases, respectively. The evaporation process we describe refers to elements escaping out of Phase I through various mechanisms, such as chemical reaction, mass transfer, and/or nucleation (see Fig. 2). And, we don't consider those M-bearing species have left the interface, as only residual M-bearing species in the melt is used to calculate KIFF in experiments (e.g., Richter et al. 2002, 2007). Chemical reactions for evaporation can either occur inside of the melt as implicated by the works

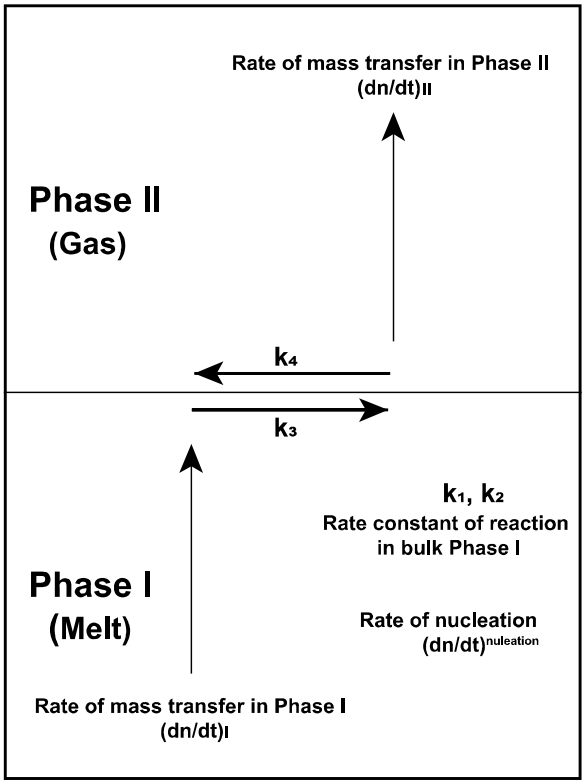

Fig. 2 The whole steps an evaporation process can experience. n is the amount of substance; (dn/dt) represents the rate of an interested element escape from Phase I; $(dn/dt)_I$ or $(dn/dt)_{II}$ is the rate of mass transfer in Phase I or II, respectively. $(dn/dt)^{nucleation}$ is the rate of nucleation. k_1 or k_2 is the rate constant of forward or reverse reaction in bulk Phase I, respectively. k_3 or k_4 is the rate constant of forward or reverse reaction at interface between Phase I and Phase II, respectively

of Townsend et al. (2020) and Caracas and Stewart (2023) or at the interface between gas and melt suggested by Hayes (2014). The mass transfer can take place anywhere due to differences in concentration.

The whole process consists of 5 reactions/steps as illustrated in Fig. 2, and each of them can influence the overall rate. Therefore, we must analyze how these reactions/steps affect the overall rate. There are three cases, i.e., mass transfer, chemical reactions, and nucleation.

2.2.1.1 Case (a): mass transfer in Phase I (i.e., silicate melt) or phase II (i.e., gas) is the rate-limiting step Firstly, given that mass transfer in silicate melts is rate-limiting, its rate in Phase I for element M is expressed as follows,

$$\left(\frac{dn}{dt}\right)_I = area \times k_{\mathrm{MI}}\left(C_I - C_I^i\right) \tag{4}$$

Secondly, if the overall evaporation process is controlled by mass transfer from interface into gas, its rate in Phase II is,

$$\left(\frac{dn}{dt}\right)_{II} = area \times k_{\mathrm{MII}}\left(C_{\mathrm{II}}^i - C_{\mathrm{II}}\right) \tag{5}$$

where k_{MI} and k_{MII} are the mass transfer coefficient of M-bearing species in Phase I or II, respectively; C_{I} or C_{I}^i denotes the concentration of M-bearing species in bulk Phase I or at interface near Phase I; Similarly, C_{II} and C_{II}^i are the concentration of M-bearing species in bulk Phase II or at interface near Phase II, respectively; area is the surface area of the sphere of experimental sample.

In this scenario, the rate of chemical reactions in bulk Phase I and at the interface is so fast that these reactions approach local equilibrium. If reactions at the interface are assumed as a first-order reaction, we can get,

$$k_3 C_{\mathrm{I}}^i = k_4 C_{\mathrm{II}}^i \tag{6}$$

$$\frac{C_{\mathrm{I}}^i}{C_{\mathrm{II}}^i} = \frac{k_4}{k_3} = k^{eq} \tag{7}$$

k_3 and k_4 are rate constants of forward and back reaction, k^{eq} is the equilibrium constant of reaction at interface.

Also, C_{II}^i is equal to C_{II} when mass transfer in Phase I is the limiting step, and C_{I}^i is equal to C_{I} for mass transfer of Phase II dominating evaporation. Then, Eqs. (4) and (5) become, respectively,

$$\left(\frac{dn}{dt}\right)_I = k_{\mathrm{MI}}\left(C_{\mathrm{I}} - C_{\mathrm{II}} k^{eq}\right) \tag{8}$$

$$\left(\frac{dn}{dt}\right)_{II} = k_{\mathrm{MII}}\left(\frac{C_{\mathrm{I}}}{k^{eq}} - C_{\mathrm{II}}\right) \tag{9}$$

In this scenario, mass transfer is slow. Theoretically, we can see the concentration gradient in the profile of silicate melt or gas phase (Sossi et al. 2020; Zhang et al. 2021).

The mass transfer in the above equation consists of advection and diffusion. If diffusion is dominant in this case, the rate of Case (a) can be described via the diffusion equation (Richter et al. 2002; Sossi et al. 2020).

2.2.1.2 Case (b): Chemical reactions in bulk phase I or at interface are the rate-limiting steps Chemical reactions can take place in bulk Phase I or at the interface separately, or both. Here we take reactions in bulk Phase I as an example to illustrate.

The rate of chemical reaction in bulk Phase I is determined by the rate constant and concentration of reactant and product. We assume that it is a decomposition reaction at such a high temperature under vacuum:

$$A = B + C \tag{10}$$

And the rate for this process is

$$-\frac{dn_A}{dt} = V\left(k_1 C_A - k_2 C_B C_C\right) \tag{11}$$

where n_A is the amount of substance of A; C_A, C_B, and C_C are the concentration for A, B, and C, respectively. V is the volume of melts. The relation between n and C is $n = CV$.

If the products B and C can be removed rapidly into vacuum, the rate is equal to Vk_1C_A. Note that this illustration for reactions in Bulk Phase I is also suitable for those at the interface.

The most significant difference between our model and the H–K equation is that chemical reactions are considered.

2.2.1.3 Case (c): nucleation The nucleation usually occurs in phase transformation. It is another fundamentally kinetic process that has been studied systematically (Carey 2020). And, we believe that evaporation of silicate also experiences the nucleation process, since it involves melts-gas transformation. The nucleation here refers to the formation of initial small species. For instance, MgO(melt) → MgO(gas) and SiO_2(melt) → SiO_2(gas).

2.2.2 Isotopic fractionation factor of our model

2.2.2.1 Isotopic fractionation factor based on case (a) For Case (a), mass transfer is the rate-limiting step, thus this process also controls KIFFs. Mass transfer goes as advection and diffusion, but till now, the diffusion process is more considered compared to advection in the field of evaporation for silicate melt.

According to Case (a), there are two scenarios, i.e., mass transfer taking place from the interface into gas or inside of silicate melt. The former process has been studied well and is connected to the H–K equation to give a net flux expression for evaporation (Richter et al. 2002; Sossi et al. 2020),

$$J_{net} = \frac{J_i\left(1-\frac{P_{i,\infty}}{P_{i,sat}}\right)}{1+\frac{\gamma_i a}{D_i}\sqrt{\frac{RT}{2\pi m_i}}} \tag{12}$$

$$J_{net} = \frac{J_i}{1+\frac{\gamma_i P}{k_c\sqrt{2\pi m_i RT}}\left(1-\exp(\xi)erfc\sqrt{\xi}\right)} \tag{13}$$

Both equations indicate that the net flux will be controlled by diffusion if the rate of species i from the interface into the surrounding gas is very slow. Its KIFF can be expressed as D_2/D_1 or $(D_2/D_1)^{2/3}$ (Richter et al. 2002; Sossi et al. 2020). In vacuum, D is proportional to the square root of the mass of evaporating species, i.e., $m^{0.5}$, and the KIFF we predict here has the same result if the species of diffusion is the same as the vaporized one.

When the mass transfer from interface into gas is the rate-limiting, the concentration at interface will be equal to that of bulk silicate melt due to fast mass transfer in silicate melt, i.e., $C_I = C_I^i$. If the reaction at interface is so rapid that it can reach local equilibrium, i.e., $\frac{C_{II}^i}{C_I^i} = \frac{1}{k^{eq}}$, where k^{eq} is the equilibrium constant of the reaction at interface. And there is no significant concentration of evaporating gas, i.e., $C_{II} \approx 0$, and no advection occurs under vacuum, so we can get an expression as follows,

$$\left(\frac{dn}{dt}\right)_{II} = \frac{2DC_I}{dk^{eq}} \tag{14}$$

where $k_{MI} = \frac{2D}{d}$ under vacuum (Niranjan 2022), d is the diameter of the sphere of experimental samples, C_I is the concentration in melt.

As the result of the equilibrium isotopic fractionation, i.e., k_1^{eq}/k_2^{eq}, approaching unit at high temperature (Urey 1947; Bigeleisen and Mayer 1947), we can derive the KIFF by Eq. (14) combined with $dn/dt = V(dC_I/dt)$ under vacuum,

$$KIFF \approx \frac{D_1}{D_2} = \sqrt{\frac{m_2}{m_1}} \tag{15}$$

The result of Eq. (15) is identical to the result of Richter et al. (2002).

In addition, when there is gas flow in a surrounding melt, mass transfer can be classified into two parts, i.e., natural convection and forced convection, based on the velocity of gas flow. It is natural convection for low velocity of gas flow, otherwise, it is forced convection. k_{MI} in Eqs. (8) and (9) is proportionate to $D^{2/3}$ for natural convection (Chilton and Colburn 1934; Wimber et al. 1977), so the KIFF is $(\mu_1/\mu_2)^{1/3}$ where μ is the reduced mass of evaporating gas and surrounding gas species (Sossi et al. 2020). The experiment of Badro et al. (2021) suggests that advection, i.e., the fast velocity of gas flow on the order of 8–10 m/s, also affects isotopic fractionation during evaporation. This is because the theory for vacuum and 1-atm (Richter et al. 2002; Sossi et al. 2020) cannot explain the observed KIFF in that experiment. However, solving isotopic fractionation caused by advection is not in the scope of our study.

In the end, it turns to mass transfer taking place inside of silicate melt is rate-limiting, thus concentration gradient should occur in a profile of melt which has been observed by experiments (e.g., Sossi et al. 2020; Zhang et al. 2021). And, some theoretical treatments employing diffusions were presented (Richter et al. 2002; Sossi et al. 2020; Zhang et al. 2021), which leads to a consequence that its KIFF is the square root of the ratio of diffusion coefficient of light and heavy isotope inside of melt. However, there are so many cases where concentration is homogeneous in melt due to fast diffusion (Richter et al. 2007, 2011;

Knight et al. 2009; Mendybaev et al. 2021), and significant disparities still occur for KIFFs taking place in this situation, meaning this is not the real cause for the disparities.

2.2.2.2 Isotopic fractionation factor based on cases (b) and (c) We stress that the H–K equation is not suitable for the system in which chemical reactions occur (Hayes 2014). In case (b) where the rate of chemical reactions is slow compared to mass transfer, the KIFFs are dominated by chemical reactions. At the same time, it is a reasonable assumption that reactions are decomposition reactions for the evaporation process under vacuum.

The multi-step sequential chemical kinetics model (MSCKM) and the transition state theory (TST) (Eyring 1935) are employed here to deal with the isotope fractionations for the chemical reactions process. TST has already been successfully used in the evaporation processes in vacuum by many researchers (e.g., Searcy and Beruto 1974; Cappa et al. 2007).

If based on the TST, an elementary (or one-step) decomposition reaction is given as

$$X \rightarrow A + B \tag{16}$$

An activated complex or transition state,$X^{\ddagger}$, will exist in the reaction process. Therefore, the elementary reaction can be represented as:

$$X \rightleftharpoons X^{\ddagger} \rightarrow A + B \tag{17}$$

Two important assumptions are made here: (i) Activated complex and reactant are in chemical equilibrium; (ii) Once the activated complex is decomposed to the product, it won't be formed in a backward way.

The TST can also lead to the rate equation of an elementary reaction, which is very similar to the flux expression equation of evaporation [Eq. (1)]. Assuming that the condensation phase is in isotopic homogeneous condition due to fast diffusion, the rate of an elementary decomposition reaction can be expressed as (Bigeleisen 1949)

$$-\frac{dX}{dt} = K\frac{Q^{\ddagger}}{Q_{rct}}\sqrt{\frac{kT}{2\pi\mu}}\frac{1}{\delta}\frac{X}{V} \tag{18}$$

where X is the amount of substance of reactant in melt; K is the transmission coefficient;$-\frac{dX}{dt}$ is the reaction rate; Q_{rct} and $Q^{\ddagger}$ are the partition functions for reactant and activated complex, respectively; k is the Boltzmann constant; T is the temperature in Kelvin; μ is the effective mass of activated complex; δ is the length of the top of the potential energy barrier; V is the volume of melts.

Equation (18) can be expressed for different isotopologues with heavy or light isotope, respectively:

$$-\frac{dX_2}{dt} = K_2\frac{Q_2^{\ddagger}}{Q_{2,rct}}\sqrt{\frac{kT}{2\pi m_{2,rct}}}\frac{1}{\delta_2}\frac{X_2}{V} \tag{19}$$

$$W - \frac{dX_1}{dt} = K_1\frac{Q_1^{\ddagger}}{Q_{1,rct}}\sqrt{\frac{kT}{2\pi m_{1,rct}}}\frac{1}{\delta_1}\frac{X_1}{V} \tag{20}$$

where μ is assumed as m_{rct} for the decomposition reaction here, $m_{1,\mathrm{rct}}$ and $m_{2,\mathrm{rct}}$ are the mass of reactant species with light and heavy isotopes, respectively. It has been further approved that, if under very high temperatures , $\delta_1 = \delta_2$ and $K_1 = K_2$ (Bigeleisen 1949). Based on Eqs. (19–20), we can get an expression:

$$\frac{dX_2}{X_2} = \frac{\frac{Q_2^{\ddagger}}{Q_1^{\ddagger}}}{\frac{Q_{2,rct}}{Q_{1,rct}}}\sqrt{\frac{m_{1,rct}}{m_{2,rct}}}\frac{dX_1}{X_1} \tag{21}$$

By comparison, the H–K equation method also can derive a very similar equation (Richter 2004):

$$\frac{dX_2}{X_2} = \frac{P_{2,sat}}{P_{1,sat}}\sqrt{\frac{m_1}{m_2}}\frac{dX_1}{X_1} \tag{22}$$

And we know that the KIFF derived from the H–K equation is $\approx \sqrt{\frac{m_1}{m_2}}$, where m_1 and m_2 are the molecular mass of vaporized species with light and heavy isotopes, respectively (Richter et al. 2002, 2007; Richter 2004). It means that the KIFF depends on the type of vaporized gas species. Similarly, based on the MSCKM, its KIFF is expressed as

$$\alpha_{\mathrm{CK}} = \frac{\frac{Q_2^{\ddagger}}{Q_1^{\ddagger}}}{\frac{Q_{2,rct}}{Q_{1,rct}}}\sqrt{\frac{m_{1,rct}}{m_{2,rct}}} = \alpha^{\ddagger eq}\sqrt{\frac{m_{1,rct}}{m_{2,rct}}} \tag{23}$$

We know that $\alpha^{\ddagger eq} \approx 1$ at sufficiently high temperature. Then,

$$\alpha_{\mathrm{CK}} \approx \sqrt{\frac{m_{1,rct}}{m_{2,rct}}} \tag{24}$$

Note that Eq. (24) is almost similar to the KIFF derived from the H–K equation, but it depends on the masses of reactant species with different isotopes.

For Case (c), its KIFF is similar to Case (b) and depends on the mass of the condensation phase like MgO(melt) or SiO_2(melt) for MgO(melt) → MgO(g) or SiO_2(melt) → SiO_2(g), respectively.

After instructing the isotopic fractionation factor based on Cases (a), (b), and (c), we try to give our description of the evaporation of silicate melts. Because silicate melts have the structure of networks, the process of evaporation often contains a series of steps, including reaction, diffusion, and nucleation,

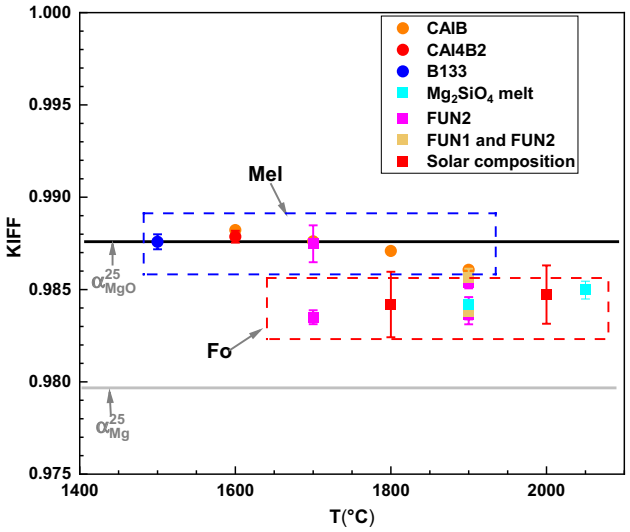

Fig. 3 KIFFs of Mg for composition and temperature under vacuum. The black or grey line represents theoretical KIFFs, i.e., α^{25}_{Mg} calculated as $(24/25)^{0.5}$ and α^{25}_{MgO} calculated as $(40/41)^{0.5}$, respectively, and the former is only predicted by the H–K equation. The results of melilitic melts (Mel) or forsteritic melts (Fo) are in blue or red squares, respectively. CAIB—from Richter et al. (2007); CAI4B2—from Mendybaev et al. (2021); B133—from Richter et al. (2002); Mg_2SiO_4 melt—from Davis et al. (1990); FUN1—from Mendybaev et al. (2013a); FUN1 and FUN2—from Mendybaev et al. (2013b); Solar composition—from Wang et al. (2001)

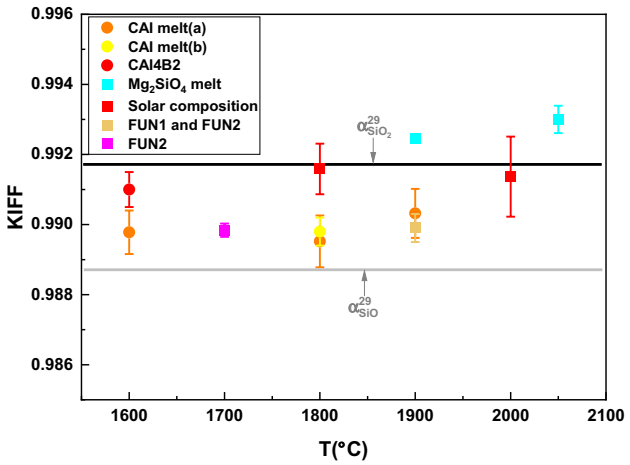

Fig. 4 KIFFs of Si for temperature and composition under vacuum. The black or grey line represents theoretical KIFFs, i.e., α^{29}_{SiO} calculated as $(44/45)^{0.5}$ and $\alpha^{29}_{SiO_2}$ calculated as $(60/61)^{0.5}$ respectively, and the former is only predicted by the H–K equation. CAI melt (**a**)—from Knight et al. (2009); CAI melt (**b**)—from Janney et al. (2005); CAI4B2–from Mendybaev et al. (2021); Mg_2SiO_4 melt—from Davis et al. (1990); Solar composition—from Wang et al. (2001); FUN1—from Mendybaev et al. (2013a); FUN1 and FUN2—from Mendybaev et al. (2013b)

$$MO_x(\text{networks or network} - \text{modifiers}) \quad \textit{breaks up, small species}(MO_1)\textit{appear} \tag{I}$$

$$MO_1 \rightarrow M + 0.5O_2 \tag{II}$$

$$MO_1\ \textit{in melt} \rightarrow MO_1\ \textit{in gas} \tag{III}$$

$$M\ \textit{in melt} \rightarrow M\ \textit{in gas}\ \infty \tag{IV}$$

where M which is vaporized species under thermodynamic equilibrium can be a single metal atom (e.g., Mg) or a multi-atomic species (e.g., SiO), whereas MO_1 is a reactant in chemical reactions like $MgO \rightarrow Mg + 0.5O_2$ and $SiO_2 \rightarrow SiO + 0.5O_2$. It is noticed that not all of these four steps are reactions. Step (I) may involve reactions and nucleation and (II) are reactions, whereas Step (III) and (IV) are mass transfer processes. For Step (I), elements are generally presented as cations that bond to oxygen to form a network structure, e.g., tetrahedra (SiO_4) and network-modifiers (e.g., Mg). Recent simulation of Caracas and Stewart (2023) showed polymers, e.g., SiO_4 and Si_2O_7, would decrease, but species SiO and SiO_2 would increase with temperature rising, indicating that the SiO_4 tetrahedra of silicate melt will break up, leading to the appearance of some small species like SiO and SiO_2 inside of melts. And we believe that the appearance of SiO_2 and SiO molecules is a result of nucleation, e.g., $SiO_2(\text{melt}) \rightarrow SiO_2(\text{gas})$, and reaction, e.g., $SiO_2 \rightarrow SiO + O$ or $0.5O_2$. The latter is Step (II) and it occurs not only inside of melts but in surrounding gas if SiO_2 escapes out of melts. Then, mass transfer of SiO_2 and SiO can take place from melt into surrounding gas, leading to the observation of them using Knudsen effusion mass spectrometry (KEMS) (Shornikov and Yakovlev 2015), which are Steps (III) and (IV). The above is a possible process inferred by simulation (Caracas and Stewart 2023).

M(melt)'s isotopic composition is a weighted average of the isotopic composition of all M-bearing components in melt that consist of tetrahedra and molecules of SiO and SiO_2 when taking Si as an example. As known, the slowest reaction step determines the rate of the overall process, then it is easy to learn that the KIFF of the overall process is controlled by the rate-limiting reaction as well, which has been used in catalysis (Liu et al. 2016). According to Eq. (24), the KIFF of an overall process is therefore:

$$\alpha_{\text{our model}} = \sqrt{\frac{m(^1\text{species of limiting step})}{m(^2\text{species of limiting step})}} \tag{25}$$

where m(species of the rate-limiting step) is the mass of the reactant for the reaction-limiting/nucleation-limiting step or species of diffusion-limiting step, so species of

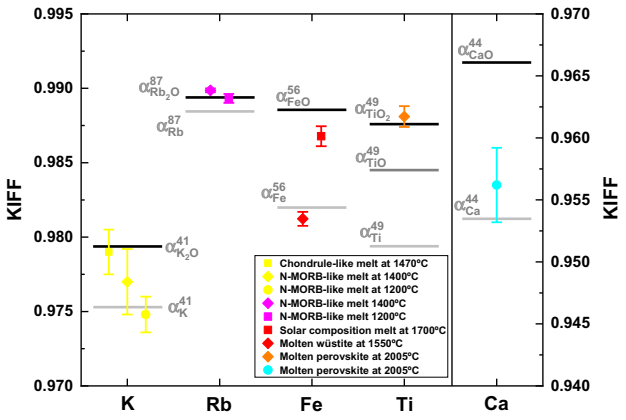

Fig. 5 Theoretical KIFFs of K, Rb, Fe, Ti, and Ca isotopes based on the H–K equation and our model compared to experiments for evaporation under vacuum. These theoretical KIFFs represented by the black or grey line, α_{K}^{41}, $\alpha_{K_2O}^{41}$, α_{Rb}^{87}, $\alpha_{Rb_2O}^{87}$, α_{Fe}^{56}, α_{FeO}^{56}, α_{Ti}^{49}, α_{TiO}^{49}, $\alpha_{TiO_2}^{49}$, α_{Ca}^{44} and α_{CaO}^{44}, are calculated as $[m(^1\text{species})/m(^2\text{species})]^{0.5}$ like $\alpha_{Ca}^{44} = (40/44)^{0.5}$ or $\alpha_{CaO}^{44} = (56/60)^{0.5}$. It should note that the H–K equation just predicts α_{K}^{41}, α_{Rb}^{87}, α_{Fe}^{56}, α_{Ti}^{49} and α_{Ca}^{44}, but all KIFFs mentioned above can be predicted by our model. Chondrule-like melt—from Richter et al. (2011); N-MORB-like melt at 1400 and 1200 °C—from Zhang et al. (2021); Solar composition; Molten wüstite—from Dauphas et al. (2004); Molten perovskite—from Zhang et al. (2014)

the rate-limiting step can be MO_1 or M, theoretically; and superscript 1 and 2 represent light and heavy isotopes, respectively.

3 Results

The KIFFs of the H–K equation are calculated as $(m_1/m_2)^{0.5}$ where m is the molecular mass of gaseous species with different isotopes. Our model's KIFFs are calculated using Eq. (25). Those experiments under vacuum and some under gas pressure are selected for comparison.

Figures 3, 4, and 5 show the comparisons of KIFFs between experiments, the H–K equation, and our model.

4 Discussion

4.1 How to diagnose kinetics of an evaporation process

Before interpreting reported KIFFs of laboratory experiments using our model, it must be made clear whether an overall evaporating process of silicate melts is controlled by diffusion, reaction, or nucleation. An equation has been

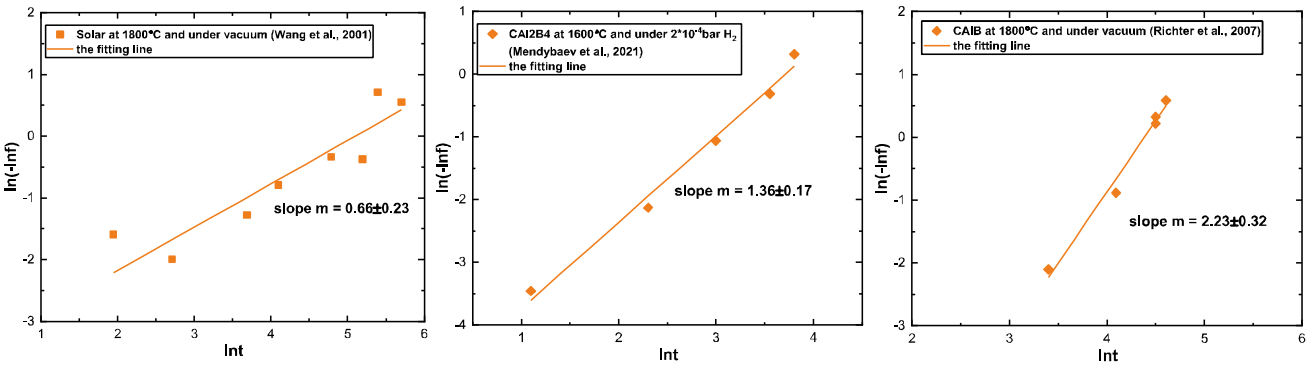

Fig. 6 Data of Mg plotted using Eq. (26). Data from Wang et al. (2001), Mendybaev et al. (2021) and Richter et al. (2007)

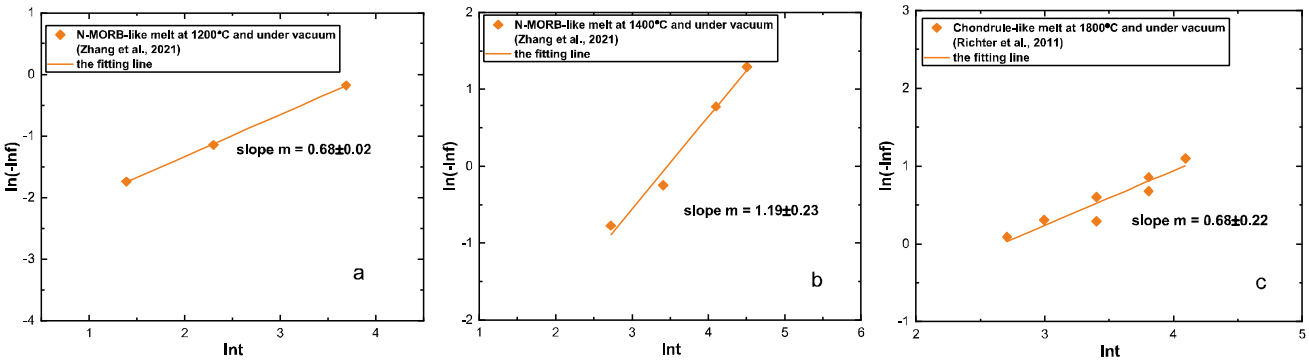

Fig. 7 Data of K plotted using Eq. (26). Data from Zhang et al. (2021) and Richter et al. (2007)

Table 1 Slopes *m*s calculated using Eq. (26) for starting materials, size, temperature and pressure

	Starting materials	Size (mm in diamter)	Temperature (°C)	Pressure	*m*	2 SE
Mg	FUN1[a]	2.5	1900	Vacuum	1.63	0.45
Mg	Solar composition[b]	6	2000	Vacuum	1.17	0.22
Mg	Solar composition[b]	6	1800	Vacuum	0.66	0.23
Mg	CAIB[c]	2.5	1900	Vacuum	2.56	1.33
Mg	CAIB[c]	2.5	1800	Vacuum	2.23	0.32
Mg	CAIB[c]	2.5	1700	Vacuum	1.63	1.55
Mg	CAIB[c]	2.5	1600	Vacuum	2.14	1.12
Mg	CAI4B2[d]	2.5	1600	Vacuum	1.71	0.49
Mg	CAI4B2[d]	2.5	1600	2×10^{-4} bar	1.37	0.17
Mg	BCAI[e]		1500	2×10^{-4} bar	1.28	1.10
Si	FUN1[f]	2.5	1900	Vacuum	2.12	0.68
Si	Solar composition[b]		2000	Vacuum	0.76	0.15
Si	Solar composition[b]		1800	Vacuum	0.65	0.13
Si	CAIB[c]	2.5	1900	Vacuum	1.18	0.21
Si	CAIB[c]	2.5	1800	Vacuum	1.11	0.27
Si	CAIB[c]	2.5	1600	Vacuum	1.14	0.52
Si	CAI4B2[d]	2.5	1600	Vacuum	1.49	0.33
Si	CAI4B2[d]	2.5	1600	2×10^{-4} bar	1.35	0.34
Si	BCAI[e]		1500	2×10^{-4} bar	1.32	0.72
K	N-MORB-like melt[f]	2.5	1400	Vacuum	1.19	0.23
K	N-MORB-like melt[f]	2.5	1200	Vacuum	0.68	0.02
K	Chondrule-like melt[g]	2.5	1470	Vacuum	0.68	0.23
Ca	Molten perovskite[h]	4	2005	Vacuum	0.77	0.08
Ti	Molten perovskite[h]	4	2005	Vacuum	0.68	0.29
Rb	N-MORB-like melt[f]	2.5	1400	Vacuum	0.78	0.11
Rb	N-MORB-like melt[f]	2.5	1200	Vacuum	0.91	0.17
Cu	PNB-like melt[i]	1	1500	1 atm, $\log fO_2 = -0.68$ and $\Delta FMQ = 4.72$	0.68	0.06
Cu	PNB-like melt[i]	1	1300	1 atm, $\log fO_2 = -0.68$ and $\Delta FMQ = 6.62$	0.97	0.02
Cu	PNB-like melt[i]	1	1400	1 atm, $\log fO_2 = -3.07$ and $\Delta FMQ = 3.2$	–0.32	0.78
Zn	PNB-like melt[i]	1	1500	1 atm, $\log fO_2 = -0.68$ and $\Delta FMQ = 4.72$	0.62	0.22
Zn	PNB-like melt[i]	1	1300	1 atm, $\log fO_2 = -0.68$ and $\Delta FMQ = 6.62$	1.04	0.06
Zn	PNB-like melt[i]	1	1400	1 atm, $\log fO_2 = -3.07$	0.44	0.74
Zn	PNB-like melt[i]	1	1400	1 atm, $\log fO_2 = -5.5$	0.45	0.55
Zn	PNB-like melt[i]	1	1500	1 atm, $\log fO_2 = -8$	0.73	0.45

[a]From Mendybaev et al. (2013a); [b]from Wang et al. (2001); [c]from Richter et al. (2007); [d]from Mendybaev et al. (2021); [e]from Richter et al. (2002); [f]from Zhang et al. (2021); [g]from Richter et al. (2011); [h]from Zhang et al. (2014); [i]from Sossi et al. (2020). N-MORB and PNB are abbreviations of normal mid-ocean ridge basalt and primitive natural basalt, respectively. Uncertainty of standard error (SE) is calculated by stats models which is one module of Python

presented to diagnose different kinetics by previous work (Sharp et al. 1966; Carter 1961; Hancock and Sharp 1972):

$$\ln(-\ln f) = lnB + mln(t) \quad (26)$$

where f is the fraction of an interested element remaining in residue after evaporation, t is evaporating time, and B and m are constants.

Three groups, i.e., the diffusion-controlled process, the phase-boundary-controlled/first-order reaction, and the reactions that obey the Avrami-Erofe'ev equation, can be distinguished according to the value of m (Hancock and Sharp 1972). If m ranges from 0.54 to 0.62, it is a diffusion-controlled process; if m is from 1.00 to 1.11, it is a phase-boundary-controlled or first-order reaction; if m is from 2.00 to 3.00, it is the Avrami-Erofe'ev equation which is used to describe the nucleation reaction (Hancock and Sharp 1972).

Previously published Mg and K data are plotted by $\ln(-\ln f)$ versus $\ln(t)$ in Figs. 6 and 7, respectively. More slopes (m) calculated using Eq. (26) are compiled in Table 1.

There are three different slopes, i.e., 0.66 ± 0.23, 1.36 ± 0.17, and 2.23 ± 0.32 (Fig. 6). It proves that evaporation for silicate melt can be limited by diffusion, reaction, or nucleation. Our model is repeatedly emphasizing this point.

In addition, we want to discuss the rationality of those kinetics from a thermodynamic view. Theoretically, the evaporation process happens when the energy exceeds the maximal activity energy (E_a) of reaction or nucleation. The reported E_a is 553 ± 32 kJ/mol and 564 ± 42 kJ/mol for Mg and Si systems under vacuum (Mendybaev et al. 2021). However, the detailed E_a for each step remains unknown. But based on the transition state theory, E_a is higher than its enthalpy of formation. For instance, the enthalpy of formation is up to 591 kJ/mol for $SiO_2(melt) \rightarrow SiO_2(gas)$ (Chase 1998). It was suggested as the limiting step by Hashimoto (1990). It is 453 kJ/mol for $SiO_2 \rightarrow SiO + O$, and 589 kJ/mol for $MgO(melt) \rightarrow MgO(gas)$ whereas 334 kJ/mol for $MgO \rightarrow Mg + O$ (Chase 1998). It is reasonable because the maximal enthalpy of formation above is lower than or close to the observed E_a indeed.

4.2 The explanations about experimental KIFFs

For magnesium isotope, the reported experimental KIFFs are closely related to the melt composition, e.g., melilitic and forsteritic melts (Fig. 3). The experimental and thermodynamic calculation both suggest the evaporating species as Mg atom for the systems including melilitic and forsteritic melt (Fedkin et al. 2006; Shornikov and Yakovlev 2015). If based on the H–K equation, the KIFF is $\alpha^{25}_{Mg} = (24/25)^{0.5} = 0.9798$ and is different from almost all experimental results, e.g., Davis et al. (1990), Richter et al. (2002, 2007) and Mendybaev et al. (2013a, b, 2021). But Davis et al. (1990) and Wang et al. (2001) found that it could match well using the H–K equation if the evaporating species was MgO, whereas this species was not supported by observation and calculation.

Here, we can give a simple and reasonable explanation. First, it is normal that mass transfer of species Mg atom also cannot explain observed results, because diffusion is not observed except the result at 1800 °C of Wang et al. (2001) (see Table 1). Table 1 shows that the rate is controlled possibly by nucleation for melilitic melts including CAIB, CAI4B2, and BCAI starting materials, whereas it could be any for forsteritic melts for Solar composition and FUN1. Meanwhile, the nucleation-limiting step [$MgO(melt) \rightarrow MgO(gas)$] and reaction-limiting step ($MgO \rightarrow Mg + 0.5O_2$) have the same predicted KIFFs based on our model, i.e., $\alpha^{25}_{MgO} = (40/41)^{0.5} = 0.9877$, which can provide key information about the kinetic mechanism of evaporation. We believe that KIFFs are the results of kinetic processes during evaporation, so slope m and KIFFs can be coupled with each other. Hence, the expected value of KIFF of nucleation $MgO(melt) \rightarrow MgO(gas)$ matches experiments of melilitic melts well. However, it does not match those of forsteritic melts (Fig. 3). For forsteritic melts, it is not the same as the evaporation of melilitic melts for which a single step can reproduce its experimental KIFFs and may encounter a little bit complex situation where both of reactions [Step (i)] and mass transfer [Step (ii)] dominate overall rate jointly, resulting in a consequence that the expected KIFF value based on our model is among two end-number, e.g., $\alpha^{25}_{Mg} = (24/25)^{0.5}$ to $\alpha^{25}_{MgO} = (40/41)^{0.5}$, with accordance of Sect. 4.4. As a result, it is reasonable for KIFFs of forsteritic melts because our model can predict it in theory. Meanwhile, we can diagnose this mechanism via slope m in Eq. (26) in principle, then there are two possibilities to interpret the ms of forsteritic melts (Table 1). The first one is that, it is nucleation-limiting or reaction-limiting for FUN1 if considering uncertainty and is reaction-limiting or diffusion-limiting for solar composition at 2000 or 1800 °C, respectively. But its expected KIFFs based on this possibility are inconsistent with experimental ones. The second one is that ms are the results of the mixing of diffusion and nucleation. Hence, we prefer the second possibility.

$$MgO(gas) \rightarrow Mg(gas) + O(gas) \quad \text{(i)}$$

$$\text{Mass transfer of Mg atom} \quad \text{(ii)}$$

For the silicon isotope system, the thermodynamic calculation and the results of KEMS both showed that the vaporized species is SiO(gas) dominantly with some SiO_2 molecules (Fedkin et al. 2006; Shornikov and Yakovlev 2015). The KIFF based on the H–K equation is $= \alpha^{30}_{SiO}$ $(44/46)^{0.5} = 0.9780$, which is not consistent with all of the experimental results (Fig. 4). In terms of our model, Table 1 shows that evaporation of CAIB and CAI4B2 seemly is controlled by chemical reaction. As we know, the predicted KIFF of reaction $SiO_2 \rightarrow SiO + O$ is $= \alpha^{30}_{SiO_2}$ $(60/62)^{0.5} = 0.9837$, and mismatch the result of either CAI4B2 or CAIB but solar composition (Fig. 4). However, the KIFFs of CAIB, CAI4B2, and FUN1 indicate a consequence of mixing of mechanisms, i.e., diffusion of species SiO and chemical reaction/nucleation. Both KIFFs and ms indicate the kinetic mechanisms, so they seem to be paradoxical. How to reconcile KIFFs and ms? One explanation is that their overall evaporation is controlled by two kinetics jointly, so these ms of CAIB, CAI4B2, and FUN1 are also among two end-numbers, whereas it is determined solely by the diffusion of species SiO_2 for solar composition. For molten Mg_2SiO_4, its KIFFs are larger than $= \alpha^{30}_{SiO_2}$

$(60/62)^{0.5} = 0.9837$ and cannot be explained and may be affected by additional recondensation processes.

For the potassium isotope system, thermodynamic calculation showed that the vaporized species is K(gas) (Fedkin et al. 2006). The KIFF based on the H–K equation is $\alpha_K^{41} = (39/41)^{0.5} = 0.9753$, which is discrepant with Richter et al. (2011) at 1470 °C, but is very close to the observed result of Zhang et al. (2021) at 1200 °C. And the result with the uncertainty of Zhang et al. (2021) at 1400 °C covers nearly from $= \alpha_K^{41}(39/41)^{0.5} = 0.9753$ to $\alpha_{K_2O}^{41} = (94/98)^{0.5} = 0.9794$. Besides the explanation of diffusion-limited evaporation based on the H–K equation (Zhang et al. 2021), we also can provide another one. The KIFFs derived from the H–K equation and mass transfer of species K atom are the same, so this mass transfer in our model explains the experiment of Zhang et al. (2021) at 1200 °C, which is proved using Eq. (26), while it is a reaction-limiting step for the experiment of Zhang et al. (2021) at 1400 °C (Table 1). However, it is diffusion-limiting for the work of Richter et al. (2011) under vacuum (Table 1), and a possible mechanism is the diffusion of species K_2O controlling the overall rate of evaporation to reconcile its KIFF and *m*. As for rubidium (Zhang et al. 2021), two *m*s (Table 1) are coupling to two KIFFs (Fig. 5), respectively, and those two KIFFs are close to $= \alpha_{Rb_2O}^{87}(186/190)^{0.5} = 0.9894$ instead of $\alpha_{Rb}^{87} = (85/87)^{0.5} = 0.9884$ (Fig. 5), meaning our model is useful again.

For the iron isotope system, the vaporized Fe-bearing species is the Fe molecule suggested by the thermodynamic calculation (Fedkin et al. 2006) and the KEMS system (Costa et al. 2017; Plante et al. 1992). So considering the H–K equation, the KIFF is $= \alpha_{Fe}^{56}(54/56)^{0.5} = 0.9820$, which is quite close to the experimental data of wüstite, but not consistent with another experiment (Fig. 5; Dauphas et al. 2004). We can give a simple explanation for this based on our model under the condition where *m* is lacking because information about evaporation time, i.e., ln*t*, is not reported in Dauphas et al. (2004). Our model can predict two KIFFs, α_{Fe}^{56} and $= \alpha_{FeO}^{56}(70/72)^{0.5} = 0.9860$ theoretically. The former requires gaseous Fe atom as the diffusion species to explain the experiment of wüstite (Dauphas et al. 2004; Fig. 5). The latter requires the nucleation [FeO(melt) → FeO(gas)] or chemical reaction (FeO → Fe + O) mechanism, which is close to the observed value of the solar composition (Dauphas et al. 2004; Fig. 5).

For the calcium isotope system, the reported KIFF from the experiment is roughly consistent with the expected value based on both the H–K equation and mass transfer as the explanation for Mg, Si, K, and Fe system (Zhang et al. 2014; Fig. 5), owing to that the vaporized species was suggested as

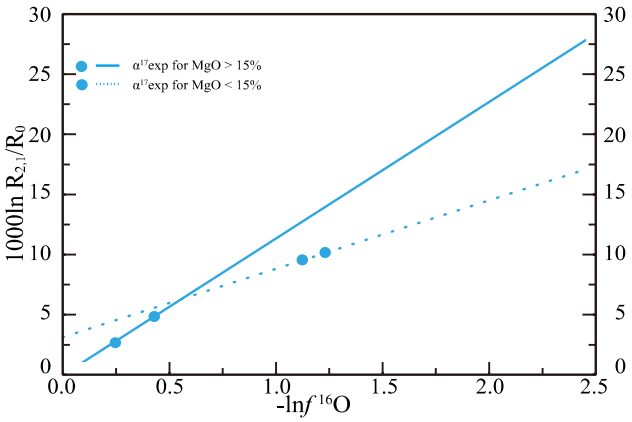

Fig. 8 O isotopic composition of the evaporation residues plotted as 1000 ln $R_{2,1}/R_0$ versus $-\ln f^{16}O$. Data are from Mendybaev et al. (2013a)

Ca atom (Shornikov and Yakovlev 2015; Shornikov 2020). Also, it is true for the titanium isotope system (Zhang et al. 2014), its KIFF also can be reproduced roughly via both the H–K equation and our model with observed evaporating species, i.e., TiO_2 (Shornikov and Yakovlev 2015; Shornikov 2020; Fig. 5). In addition, both of Ca and Ti system are controlled by diffusion of vaporized species (Table 1), leading to the same KIFFs predicted with both the H–K equation and our model.

For the oxygen isotope system, there is an obvious phenomenon that there are two different slopes in "$1000\ln\frac{R_{2,1}}{R_0}$ versus $-\ln f$" for one evaporation experiment, which is similar to Mg isotopic system (Mendybaev et al. 2013a, b; Fig. 8). We propose that it is another sign of evidence for our model, because our model predicts a coupling change between Mg and O isotopic factor, referring that the KIFF of O can vary with the variation of the KIFF of Mg. First, Mg is present as the form of MgO(melt or gas) and Mg(gas) and the *F* in Eq. (27) of the step involving MgO can be different for different compositions, i.e., MgO > 15 wt% and MgO < 15 wt%. Then, the step involving MgO changes Mg and O isotope fractionations together. Thus, this phenomenon can be predicted according to Eqs. (24 and 27).

4.3 Cases cannot be explained

Besides evaporating experiments of silicate melt under vacuum (near vacuum) and low P_{H2}, there are others performed under higher ambient pressure or different oxygen fugacity controlled by gas composition mixture, e.g., Ar, He, CO–CO_2, and Air, and flow rate. The KIFFs of Cu, Zn, K,

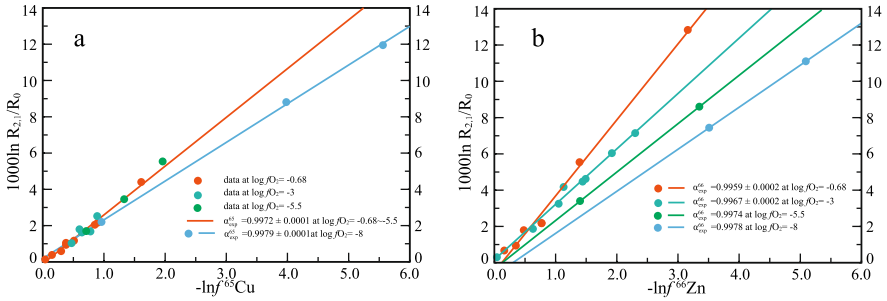

Fig. 9 Cu and Zn isotopic composition of the evaporation residues plotted as 1000ln $R_{2,1}/R_0$ versus $-\ln f^{1}X$ where ^{1}X represents ^{63}Cu or ^{64}Zn. Data are from Sossi et al. (2020)

Cr, Te, Si, and Mg have been reported (Yu et al. 2003; Richter et al. 2011; Ni et al. 2021; Wimpenny et al. 2019; Sossi et al. 2020; Neuman et al. 2022; Renggli et al. 2022; Young et al. 2022; Badro et al. 2021). These experiments cannot be matched by both the H–K equation and our model under vacuum. Taking the result of Sossi et al. (2020) as an example, $\alpha^{65}_{Cu,exp}$ and $\alpha^{66}_{Zn,exp}$ are different from those theoretically predicted based on different vaporized species, such as $\alpha^{65}_{Cu} = 0.9845, \alpha^{65}_{CuO} = 0.9876, \alpha^{65}_{Cu_2O} = 0.9862, \alpha^{66}_{Zn} = 0.9847$, and $\alpha^{66}_{ZnO} = 0.9877$, etc. Our model also cannot explain them (Fig. 9). These experiments were performed under conditions that are far away from the vacuum, e.g., with a gas flow of air, Ar, etc. They do not meet the requirements of either our model or the H–K equation. But that can be interpreted by diffusion using $(\mu_1/\mu_2)^{1/3}$ that was developed by Sossi et al. 2020 where μ is the reduced mass of vaporized species and surrounding gas. It was considered a diffusion-limiting region because concentration zoning was observed (Sossi et al. 2020). Using Eq. (26), most obtained *m*s of Cu or Zn are quite close to the value of diffusion except one under the condition of $\log fO_2 = -0.68$ and $\Delta FMQ = 6.62$ (Table 1), so this is another evidence of diffusion controlling evaporation of this case. But this formula, $(\mu_1/\mu_2)^{1/3}$, is defective because it cannot explain the KIFF of Zn under the gas flow of Ar (Sossi et al. 2020). Therefore, future modifications of our model are necessary to reproduce these experimental KIFFs of Zn and Cu mentioned here. The goal of those theoretical considerations is to make the current version of our model become one that can be suitable for conditions far away from a vacuum. One important theoretical consideration is to add other components, such as H_2, CO_2, S, Cl, N, and so on to evaluate the effects of different kinetic mechanisms, which may be different from those under vacuum conditions.

4.4 The KIFFs-mixing model

Though our model can explain more the experimental KIFFs than the H–K equation under vacuum till now, there are still so many other phenomena to be discussed, such as composition, temperature, and low P_{H2} effects (Richter et al. 2002, 2007; Dauphas et al. 2004; Zhang et al. 2021; Mendybaev et al. 2021). Although we have employed our model to give a simple explanation for the observed KIFFs, e.g., Mg, K, Si, Ca, Ti, and Fe isotope systems, a more detailed description is proposed as follows,

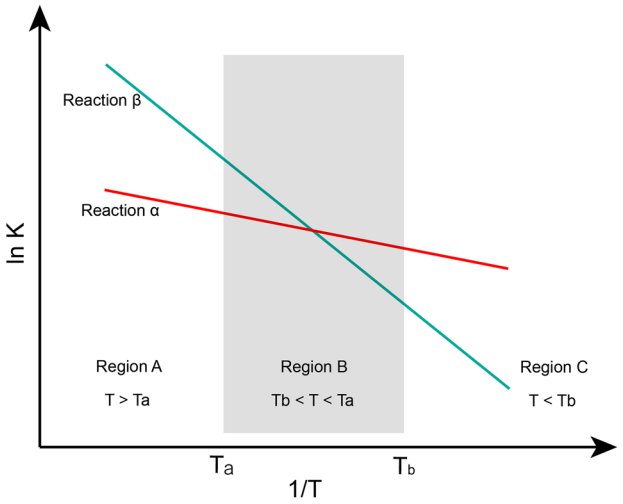

Fig. 10 Two lines based on Arrhenius equation. Three regions can be divided by temperature, i.e., Region A ($T > T_a$), Region B ($T_b < T < T_a$), and Region C ($T < T_b$)

For a chemical process, as the result that it can experience many steps, each step has its pre-exponential factor (A) and activation energy (E_a) according to the Arrhenius equation expressed as $k = A\exp(-E_a/RT)$ or $\ln k = \ln A - E_a/RT$. The simplest situation is that only one single step, the slowest step, controls the overall rate, which can explain the KIFFs of K, Ca, Ti, and Fe systems. For Mg and Si systems, a more complex situation where at least two steps both control the overall rate simultaneously should be invoked. An arbitrary line in based on the Arrhenius equation can be determined by two parameters, i.e., A and E_a. And two lines will

intersect if their E_a are different. Three regions can be classified by temperature in Fig. 10 i.e., Region A ($T > T_a$), Region B ($T_b < T < T_a$), and Region C ($T < T_b$). Reaction α or β controls the overall rate in Region A or C, respectively, whereas both Reaction α and β jointly control that in Region B. As temperature can affect the rate constant significantly, there must be a situation where the overall rate can be determined by both two reactions together within a certain temperature range, i.e., Region B. Therefore, under this condition, the KIFF can be expressed via a two end-member mixing model,

$$KIFF = F_\alpha w_\alpha + \left(1 - F_\alpha\right) w_\beta \quad (27)$$

where w_α or w_β are the KIFFs at certain T and F_α is the fraction of the w_α. Then, if $T > T_a$ or $T < T_b$, the overall process will be controlled by a single reaction owing to the very large difference between two rate constants (Fig. 10). We name this the KIFFs-mixing model.

The composition and temperature effects can be explained by the KIFFs-mixing model.

Because the relation in Fig. 10 is just suitable for chemical reactions, we assume that the diffusion coefficient and the constant in the nucleation process also can be described by the Arrhenius equation. The basic physical meaning is not lacking, though conditions are simplified.

4.5 The explanations for effects of composition, temperature, and low-P_{H2}

4.5.1 Composition effect

Mendybaev et al. (2013a, b) found that KIFFs of Mg and O will vary from residues with more than 15 wt% MgO (i.e., forsteritic melts) into one with less than 15 wt% MgO (i.e., melilitic melts), but KIFF of Si doesn't vary. It is called as composition effect here. The reason for the phenomena of Mg and Si can be described by the KIFFs-mixing model. The slope *m*s in Eq. (26) for melilitic melts (Table 1; see the discussion in Sect. 4.2) suggests that this evaporation process takes place in Region A or C dominantly, whereas the case for forsteritic melts is controlled by both nucleation and mass transfer, so it belongs to Region B dominantly. Therefore, their KIFFs vary naturally from Region A or C into Region B with melt composition varying. The reason why KIFF of Si doesn't vary is that its region is unchanged and is in Region B dominantly when melt composition is changed (see the discussion in Sect. 4.2).

4.5.2 Temperature effect

The temperature effect found firstly by Richter et al. (2007) is that the KIFFs of Mg will change with temperature, while the KIFFs of Si cannot (Knight et al. 2009). And, its temperature effect can be readily predicted based on the KIFFs-mixing model if the contribution of mass transfer, F in Eq. (27), slightly increases with temperature rising in Region A or C for the Mg system because the change of its KIFF just is slight and its value still is close to α^{25}_{MgO} in general, whereas F does not increase with temperature in Region B for Si systems. Theoretically, we also can obtain a slight change of m, but it could be indistinguishable experimentally considering uncertainty (see Table 1).

4.5.3 Low-P_{H2} effect

Experiments by Richter et al. (2002) and Mendybeav et al. (2021) found that low-P_{H2} can increase the evaporating rate but have no influence on KIFFs for both Mg and Si. They gave a reasonable explanation that saturation vapor pressures of Mg and SiO species in the H–K equation increase with hydrogen pressure as $\sqrt{P_{H2}}$, so resulting in increasing the rate with P_{H2}. However, it still cannot explain the phenomenon of no variation of KIFFs. Here we try to give a possible explanation from the view of our model. For Mg, the kinetic is nucleation-limiting under vacuum and becomes reaction-limiting under low P_{H2} pressure (Table 1), and H_2 may increase the frequency of molecular collisions, resulting in acceleration of the reaction rate. Then, we know KIFFs of nucleation and decomposition of MgO are the same. Hence, we think it is the mechanism for the low-P_{H2} effect for Mg. For Si, m is about 1 (Table 1) both under vacuum and low-P_{H2}, and the explanation for Mg is invalid for Si, thus it needs another interpretation. We guess that the reaction $0.5O_2$ or $O + H_2 \rightarrow H_2O$ can consume O or O_2 in reaction $SiO_2 \rightarrow SiO + O$ or $0.5O_2$, so that the rate of decomposition of SiO_2 is increasing but its KIFF is not changed, since its mechanism does not vary and just the product of O or O_2 is consumed (Eq. 11).

4.6 Vapor saturation approaches zero under vacuum

$$\Delta = \Delta_{eq} + (1 - S)\Delta_{kin} \quad (28)$$

The vapor saturation S can be determined by this equation where $\Delta = \alpha - 1$; α is the experimental KIFF, i.e., α_{exp}, equilibrium isotope fractionation factor, i.e., α_{eq}, or KIFF based on the H–K equation, i.e., α_{kin}, for Δ, Δ_{eq} or Δ_{kin}, respectively; α_{eq} is close to 1 under high temperatures; α_{kin} is $(m_1/m_2)^{0.5}$ where m is the mass of gaseous species with isotopes; $S = P_i/P_{i,sat}$ where P_i is the vapor pressure at the evaporating surface and $P_{i,sat}$ is saturation vapor pressure; Eq. (28) is derived from the H–K equation (Richter et al. 2002; Dauphas et al. 2015).

There is an observation that the vapor saturation S calculated as Eq. (28) is larger than zero for most experiments (Davis et al. 1990; Richter et al. 2002, 2007; Wang

et al. 2001; Mendybaev et al. 2013a, b, 2021) except Fe, Ca, and K (Dauphas et al. 2004; Zhang et al. 2014, 2021) under vacuum. It means that experiments performed under vacuum (i.e., S close to zero) lead to a consequence of nonvacuum calculated as Eq. (28) (i.e., S is significantly larger than zero). For instance, the vapor saturation ranges from 0.31 to 0.42 for experiments of Richter et al. (2007) at 1600–1900 °C under vacuum. Our model can address this problem, i.e., S is close to zero relatively ($S=-0.14$ to 0.04) if theoretical kinetic α_{kin} equals 0.9877 predicted by the decomposition reaction of MgO or nucleation.

4.7 Implications

1. CAIs are the oldest solids (Connelly et al. 2012) in the solar system, so it is suggested as a good object to study the formation and evolution of the early solar system. One feature is experiencing evaporation and condensation processes (Clayton et al. 1988; Davis et al. 1990). However, there are lots of unclear details. For instance, what is the precursor of CAIs, and how to know those conditions or processes (e.g., pressure, cooling rate, and heating time) quantitatively? Addressing those questions can help us learn the history of the early solar system. Thus, an indispensable thing is to build a relationship between the rate of evaporation or KIFFs and those conditions such as composition, temperature, and pressure, which was performed by laboratory experiments and conventional theory before. For conventional theory on evaporation, the H–K equation has been employed, but it cannot explain many reported isotopic results of evaporation experiments (Richter et al. 2007, 2011; Knight et al. 2009; Mendybaev et al. 2021). In this study, the model we present can overcome that problem. Therefore, we can also study the proto-solar system through theoretical calculation based on our model, while the H–K equation cannot make it because the evaporation coefficient is an empirical parameter and there is no way to access it via theoretical calculation. Our model predicts that the KIFF is determined by the rate-limiting step, so the goal is to obtain it by calculation. For example, we can search the transition state for an elementary reaction through the first-principles calculation software. Then, the limiting step can readily be recognized by comparing the rate according to activation energy and pre-exponential factor of a series of elementary reactions of interest. Therefore, we provide another theoretical method to study the evaporation process. In terms of CAIs, no matter what is mass transfer, chemical reaction, or nucleation, once their rate constants can be acquired through theoretical calculation, the kinetic mechanism is also known, leading to the determination of the overall rate and KIFF of evaporation. Finally, we can apply it to address those problems about CAIs in the end.
2. Another potential application is to study the formation and evolution of the Earth-Moon system. Abundances of many moderately volatile element and their isotopic fractionation between the Moon and Earth are distinct, which can infer isotopic fractionation factors, e.g., 0.9996 ± 0.0001 for Zn, 0.9994 ± 0.0003 for Cu and 0.9998 ± 0.0001 for K, assuming following Rayleigh distillation model (e.g., Lock et al. 2020; Wang and Jacobsen 2016; Wang and Becker 2015; Taylor and Wieczorek 2014; Paniello et al. 2012; Nie and Dauphas 2019), then one possible explanation is evaporation (e.g., Wang and Jacobsen 2016; Wang et al. 2021). A series of evaporation experiments have been done, but none reproduces those observed isotopic fractionation factors, i.e., the results of all experiments are lower than those observed values (Wimpenny et al. 2019; Sossi et al. 2020; Neuman et al. 2022). It leads to puzzles as to why is hard to interpret well those observed KIFFs via today's laboratory experiments, and whether it can be addressed by theoretical calculation. However, theoretical calculation is lacking now and can play a significant role undoubtfully, so it is quite important to develop a theoretical model that can guide us to study via calculation. Therefore, our theoretical model may be a possible tool to give some interpretations in the future. Theory till now is incapable, but it is possible if we improve our model continually. An eventual model that can simulate real natural conditions such as nonvacuum, size of a planet, and recondensation, can provide a reasonable constraint for the formation of the Earth-Moon system.

5 Conclusions

The well-accepted isotope fractionation theory, which is based on the Hertz–Knudsen equation, is improper for explaining experimental data on the evaporation of silicate melts. The reason why we propose this is that the factual situation where the evaporating species is not identical to one in the melt is not suitable for the scope of the H–K equation. Then we present a model and it can explain well the most reported results compared to the H–K equation. We point out that one advantage the H–K equation doesn't have is that our model can be performed by theoretical calculation. In addition, we find that the chemical reaction indeed can control the overall rate of the evaporation process, which is important for our model. At the same time, diffusion and nucleation also are found to be able to dominate the overall rate by plotting data on $\ln(-\ln f)$ versus $\ln(t)$. In the end,

our model has potential applications in the formation and evolution of the early solar system and Earth-Moon system.

Acknowledgements This paper is supported by Chinese NSF project (42,130,114), the strategic priority research program (B) of CAS (XDB41000000), the pre-research Project on Civil Aerospace Technologies No. D020202 funded by Chinese National Space Administration (CNSA) and Guizhou Provincial 2021 Science and Technology Subsidies (No. GZ2021SIG).

Author contributions Yun Liu selected topics and reviewed and revised the first draft; Jie Wang conceived and designed the methods, calculated data, analyzed and compiled the first draft.

Data availability All data and models used during the study appear in the submitted article.

Declarations

Conflict of interest The authors declare that they have no competing interests.

References

Badro J, Sossi PA, Deng ZB, Borensztajn S, Wehr N, Ryerson FJ (2021) Experimental investigation of elemental and isotopic evaporation processes by laser heating in an aerodynamic levitation furnace. CR Geosci. 353:101–114.

Bigeleisen J (1949) The relative reaction velocities of isotopic molecules. J Chem Phys. 17:675–678.

Bigeleisen J (1961) Statistical mechanics of isotope effects on the thermodynamic properties of condensed systems. J Chem Phys. 34:1485–1493.

Bigeleisen J, Mayer MG (1947) Calculation of equilibrium constants for isotopic exchange reactions. J Chem Phys. 15:261–267.

Bourdon B, Fitoussi C (2020) Isotope fractionation during condensation and evaporation during planet formation processes. ACS Earth Space Chem. 4:1408–1423.

Cappa CD, Smith JD, Drisdell WS, Saykally RJ, Cohen RC (2007) Interpreting the H/D isotope fractionation of liquid water during evaporation without condensation. J Phys Chem C. 111:7011–7020.

Caracas R, Stewart ST (2023) No magma ocean surface after giant impacts between rocky planets. Earth Planet Sci Lett. 608:118014.

Carey VP (2020) Liquid-Vapor Phase-Change Phenomena: An introduction to the thermophysics of vaporization and condensation processes in heat transfer equipment. Third Edition ed. CRC Press, Boca Raton.

Carter RE (1961) Kinetic model for solid-state reactions. J Chem Phys. 34:2010–2015.

Chase M (1998) NIST-JANAF thermochemical tables, 4th edn. American Institute of Physics, College Park.

Chilton TH, Colburn AP (1934) Mass transfer (absorption) coefficients prediction from data on heat transfer and fluid friction. Ind Eng Chem. 26:1183–1187.

Clayton RN, Hinton RW, Davis AM, Runcorn SK, Turner G, Woolfson MM (1988) Isotopic variations in the rock-forming elements in meteorites. Philos Trans R Soc Lond Ser A Math Phys Sci. 325:483–501.

Connelly JN, Bizzarro M, Krot AN, Nordlund A, Wielandt D, Ivanova MA (2012) The absolute chronology and thermal processing of solids in the solar protoplanetary disk. Science. 338:651–655.

Costa GCC, Jacobson NS, Fegley B Jr (2017) Vaporization and thermodynamics of forsterite-rich olivine and some implications for silicate atmospheres of hot rocky exoplanets. Icarus. 289:42–55.

Dauphas N, Janney PE, Mendybaev RA, Wadhwa M, Richter FM, Davis AM, van Zuilen M, Hines R, Foley CN (2004) Chromatographic separation and multicollection-ICP-MS analysis of iron. Investigating mass-dependent and -independent isotope effects. Anal Chem. 76:5855–5863.

Dauphas N, Poitrasson F, Burkhardt C, Kobayashi H, Kurosawa K (2015) Planetary and meteoritic Mg/Si and δ^{30}Si variations inherited from solar nebula chemistry. Earth Planet Sci Lett. 427:236–248.

Davis AM, Hashimoto A, Clayton RN, Mayeda TK (1990) Isotope mass fractionation during evaporation of Mg_2SiO_4. Nature. 347:655–658.

Eyring H (1935) The activated complex in chemical reactions. J Chem Phys. 3:107–115.

Fedkin AV, Grossman L, Ghiorso MS (2006) Vapor pressures and evaporation coefficients for melts of ferromagnesian chondrule-like compositions. Geochim Cosmochim Acta. 70:206–223.

Grossman L, Ebel DS, Simon SB, Davis AM, Richter FM, Parsad NM (2000) Major element chemical and isotopic compositions of refractory inclusions in C_3 chondrites: The separate roles of condensation and evaporation. Geochim Cosmochim Acta. 64:2879–2894.

Grossman L, Simon SB, Rai VK, Thiemens MH, Hutcheon ID, Williams RW, Galy A, Ding T, Fedkin AV, Clayton RN, Mayeda TK (2008) Primordial compositions of refractory inclusions. Geochim Cosmochim Acta. 72:3001–3021.

Hancock JD, Sharp JH (1972) Method of comparing solid-state kinetic data and its application to the decomposition of kaolinite, brucite, and $BaCO_3$. J Am Ceram Soc. 55:74–77.

Hashimoto A (1990) Evaporation kinetics of forsterite and implications for the early solar nebula. Nature. 347:53–55.

Hayes P (2014) Chapter 4.2-reaction kinetics. In: Seetharaman S (ed) Treatise on process metallurgy. Elsevier, Boston, pp 817–829.

Hertz H (1882) Ueber die verdunstung der flüssigkeiten, insbesondere des quecksilbers, im luftleeren raume. Ann Phys. 253:177–193 (**in German**).

Hirth JP, Pound GM (1963) Condensation and evaporation; nucleation and growth kinetics. Pergamon Press, Oxford.

Hu JY, Dauphas N, Tissot FLH, Yokochi R, Ireland TJ, Zhang Z, Davis AM, Ciesla FJ, Grossman L, Charlier BLA, Roskosz M, Alp EE, Hu MY, Zhao J (2021) Heating events in the nascent solar system recorded by rare earth element isotopic fractionation in refractory inclusions. Sci Adv. 7:2962.

Janney P, Richter F, Davis A, Mendybaev R, Wadhwa M (2005) Silicon isotope ratio variations in CAI evaporation residues measured by laser ablation multicollector ICP-MS.

Kennardk EH (1938) Kinetic theory of gases, with an introduction to statistical mechanics. McGraw-Hill book Company Inc., New York.

Knight KB, Kita NT, Mendybaev RA, Richter FM, Davis AM, Valley JW (2009) Silicon isotopic fractionation of CAI-like vacuum evaporation residues. Geochim Cosmochim Acta. 73:6390–6401.

Knudsen M (1909) Die gesetze der molekularströmung und der inneren reibungsströmung der gase durch röhren. Ann Phys. 333:75–130 (**in German**).

Langmuir I (1913) The vapor pressure of metallic tungsten. Phys Rev. 2:329–342.

Liu PX, Zhao Y, Qin RX, Mo SG, Chen GX, Gu L, Chevrier DM, Zhang P, Guo Q, Zang DD, Wu BH, Fu G, Zheng NF (2016)

Photochemical route for synthesizing atomically dispersed palladium catalysts. Science. 352:797–801.
Lock SJ, Bermingham KR, Parai R, Boyet M (2020) Geochemical constraints on the origin of the Moon and preservation of ancient terrestrial Heterogeneities. Space Sci Rev. 216: 109.
Luo H, Bao H, Yang Y, Liu Y (2018) Theoretical calculation of equilibrium Mg isotope fractionation between silicate melt and its vapor. Acta Geochim. 37:655–662.
Mendybaev RA, Richter FM, Georg RB, Janney PE, Spicuzza MJ, Davis AM, Valley JW (2013a) Experimental evaporation of Mg- and Si-rich melts: implications for the origin and evolution of FUN CAIs. Geochim Cosmochim Acta. 123:368–384.
Mendybaev RA, Kamibayashi M, Teng F-Z, Savage PS, Georg RB, Richter FM, Tachibana S (2021) Experiments quantifying elemental and isotopic fractionations during evaporation of CAI-like melts in low-pressure hydrogen and in vacuum: constraints on thermal processing of CAIs in the protoplanetary disk. Geochim Cosmochim Acta. 292:557–576.
Mendybaev RA, Teng FZ, Georg RB (2013b) Richter FM magnesium and silicon isotopic fractionations during evaporation of forsterite-rich melts: The temperature and composition effects.
Neuman M, Holzheid A, Lodders K, Fegley B, Jolliff BL, Koefoed P, Chen H, Wang K (2022) High temperature evaporation and isotopic fractionation of K and Cu. Geochim Cosmochim Acta. 316:1–20.
Ni P, Macris CA, Darling EA, Shahar A (2021) Evaporation-induced copper isotope fractionation: Insights from laser levitation experiments. Geochim Cosmochim Acta. 298:131–148.
Nie NX, Dauphas N (2019) Vapor drainage in the protolunar disk as the cause for the depletion in volatile elements of the moon. Astrophys J Lett. 884:L48.
Nie NX, Chen X-Y, Hopp T, Hu JY, Zhang ZJ, Teng F-Z, Shahar A, Dauphas N (2021) Imprint of chondrule formation on the K and Rb isotopic compositions of carbonaceous meteorites. Sci Adv. 7(49):abl3929.
Niranjan K (2022) Elements of mass transfer. In: Niranjan K (ed) Engineering principles for food process and product realization. Springer, Cham, pp 81–102.
Paniello RC, Day JMD, Moynier F (2012) Zinc isotopic evidence for the origin of the Moon. Nature. 490:376–379.
Plante E, Hastie J, Kowalska M (1992) Activity of FeO in the FeO-MgO-SiO_2 system determined by high temperature mass spectrometry. ISIJ Int. 32:1276–1279.
Renggli CJ, Hellmann JL, Burkhardt C, Klemme S, Berndt J, Pangritz P, Kleine T (2022) Tellurium isotope fractionation during evaporation from silicate melts. Geochim Cosmochim Acta. 339:35–45.
Richter FM (2004) Timescales determining the degree of kinetic isotope fractionation by evaporation and condensation. Geochim Cosmochim Acta. 68:4971–4992.
Richter FM, Davis AM, Ebel D, Hashimoto A (2002) Elemental and isotopic fractionation of type B calcium-, aluminum-rich inclusions: experiments, theoretical considerations, and constraints on their thermal evolution. Geochim Cosmochim Acta. 66:521–540.
Richter FM, Janney PE, Mendybaev RA, Davis AM, Wadhwa M (2007) Elemental and isotopic fractionation of Type B CAI-like liquids by evaporation. Geochim Cosmochim Acta. 71:5544–5564.
Richter FM, Mendybaev RA, Christensen JN, Ebel D, Gaffney A (2011) Laboratory experiments bearing on the origin and evolution of olivine-rich chondrules. Meteorit Planet Sci. 46:1152–1178.
Searcy AW, Beruto D (1974) Transition state theory for vaporization and condensation. J Phys Chem. 78:1298–1304.
Sharp JH, Brindley GW, Achar BNN (1966) Numerical data for some commonly used solid state reaction equations. J Am Ceram Soc. 49:379–382.
Shornikov SI (2020) Study of CaO–TiO_2 melts by knudsen effusion mass spectrometry. Russ J Phys Chem A. 94:1289–1299.
Shornikov SI, Yakovlev OI (2015) Study of complex molecular species in the gas phase over the CaO–MgO–Al_2O_3–TiO_2–SiO_2 system. Geochem Int. 53:690–699.
Sossi PA, Moynier F, Treilles R, Mokhtari M, Wang X, Siebert J (2020) An experimentally-determined general formalism for evaporation and isotope fractionation of Cu and Zn from silicate melts between 1300 and 1500 °C and 1 bar. Geochim Cosmochim Acta. 288:316–340.
Taylor GJ, Wieczorek MA (2014) Lunar bulk chemical composition: A post-gravity recovery and interior laboratory reassessment. Philos Trans R Soc Math Phys Eng Sci. 372:20130242.
Townsend JP, Shohet G, Cochrane KR (2020) Liquid-vapor coexistence and critical point of Mg_2SiO_4 from Ab initio simulations. Geophys Res Lett. 47(17):2020089599.
Urey HC (1947) The thermodynamic properties of isotopic substances. J Chem Soc (Resumed). https://doi.org/10.1039/JR9470000562,562-581
Wang Z, Becker H (2015) Abundances of Ag and Cu in mantle peridotites and the implications for the behavior of chalcophile elements in the mantle. Geochim Cosmochim Acta. 160:209–226.
Wang K, Jacobsen SB (2016) Potassium isotopic evidence for a high-energy giant impact origin of the moon. Nature. 538:487–490.
Wang JH, Davis AM, Clayton RN, Mayeda TK, Hashimoto A (2001) Chemical and isotopic fractionation during the evaporation of the FeO-MgO-SiO_2-CaO-Al_2O_3-TiO_2 rare earth element melt system. Geochim Cosmochim Acta. 65:479–494.
Wang W, Li C-H, Brodholt JP, Huang S, Walter MJ, Li M, Wu Z, Huang F, Wang S-J (2021) Sulfur isotopic signature of earth established by planetesimal volatile evaporation. Nat Geosci. 14:806–811.
Wimber RT, Hills SW, Wahl NK, Tempero CR (1977) Kinetics of evaporation/oxidation of iridium. Metall Trans A. 8:193–199.
Wimpenny J, Marks N, Knight K, Rolison JM, Borg L, Eppich G, Badro J, Ryerson FJ, Sanborn M, Huyskens MH, Yin QZ (2019) Experimental determination of Zn isotope fractionation during evaporative loss at extreme temperatures. Geochim Cosmochim Acta. 259:391–411.
Young ED, Macris CA, Tang H, Hogan AA, Shollenberger QR (2022) Isotope velocimetry: experimental and theoretical demonstration of the potential importance of gas flow for isotope fractionation during evaporation of protoplanetary material. Earth Planet Sci Lett. 589:117575.
Yu Y, Hewins RH, Alexander CMO, Wang J (2003) Experimental study of evaporation and isotopic mass fractionation of potassium in silicate melts. Geochim Cosmochim Acta. 67:773–786.
Zhang J, Huang S, Davis AM, Dauphas N, Hashimoto A, Jacobsen SB (2014) Calcium and titanium isotopic fractionations during evaporation. Geochim Cosmochim Acta. 140:365–380.
Zhang ZJ, Nie NX, Mendybaev RA, Liu M-C, Hu JJ, Hopp T, Alp EE, Lavina B, Bullock ES, McKeegan KD, Dauphas N (2021) Loss and isotopic fractionation of alkali elements during diffusion-limited evaporation from molten silicate: Theory and experiments. ACS Earth Space Chem. 5:755–784.